



OPEN

Augmented human thermal discomfort in urban centers of the Arabian Peninsula

Safi Ullah^{1,2}, Abdullah Aldossary^{2,3}, Waheed Ullah⁴ & Sami G. Al-Ghamdi^{1,2}✉

Anthropogenic climate change has amplified human thermal discomfort in urban environments. Despite the considerable risks posed to public health, there is a lack of comprehensive research, evaluating the spatiotemporal changes in human thermal discomfort and its characteristics in hot-hyper arid regions, such as the Arabian Peninsula (AP). The current study analyzes spatiotemporal changes in human thermal discomfort categories and their characteristics in AP, using the newly developed high-resolution gridded ERA5-HEAT (Human thErMAl comforT) dataset for the period 1979–2022. In addition, the study assesses the interplay between the Universal Thermal Climate Index (UTCI) and El Niño-Southern Oscillation (ENSO) indices for the study period. The results reveal a significant increase in human thermal discomfort and its characteristics, with higher spatial variability in the AP region. The major urban centers in the southwestern, central, and southeastern parts of AP have experienced significant increases in human thermal discomfort (0.4–0.8 °C), with higher frequency and intensity of thermal stress during the study period. The temporal distribution demonstrates a linear increase in UTCI indices and their frequencies and intensities, particularly from 1998 onward, signifying a transition towards a hotter climate characterized by frequent, intense, and prolonged heat stress conditions. Moreover, the UTCI and ENSO indices exhibit a dipole pattern of correlation with a positive (negative) pattern in the southwestern (eastern parts) of AP. The study's findings suggest that policymakers and urban planners need to prioritize public health and well-being in AP's urban areas, especially for vulnerable groups, by implementing climate change adaptation and mitigation strategies, and carefully designing future cities to mitigate the effects of heat stress.

Keywords Universal Thermal Climate Index (UTCI), ERA5-HEAT, Thermal discomfort, Urban centers, Arabian Peninsula (AP)

Human thermal comfort refers to the state where individuals feel satisfied or comfortable with their surrounding thermal environment^{1,2}. The intertwining impacts of climate change and rapid urbanization have significantly altered the thermal dynamics of urban environments, posing substantial challenges related to heat stress and thermal comfort^{3,4}. As global temperatures continue to rise, urban areas experience amplified heat stress or discomfort due to urban heat island (UHI) effects, characterized by increased temperature and altered urban microclimates^{5,6}. In UHI, urban areas are relatively experiencing higher temperatures than their surrounding rural areas, which is influenced by two main factors, i.e., impermeable surfaces and albedo. The proliferation of impermeable surfaces, such as asphalt and concrete, absorb and radiate heat, creating localized warming and heat stress⁶. Albedo, on the other hand, is a measure of how much sunlight is reflected by a surface, and thus low albedo surfaces or dark surfaces, like asphalt and roofs, absorb more sunlight and heat up, affecting the overall thermal comfort level in urban areas⁷. Urbanization also leads to the loss of green spaces, reducing the cooling effect of vegetation and exacerbating the heat stress and thermal discomfort in urban areas⁸. The resultant human thermal discomfort poses a multifaceted challenge, affecting both indoor and outdoor urban environments. The increase in human thermal discomfort also leads to adverse impacts on human health, labor, ecosystems, and the overall economy^{9–12}. The increasing tendency of human thermal discomfort, with profound and multifaceted consequences, underscores the need for both mitigation and adaptation strategies. Timely and accurate assessment

¹Environmental Science and Engineering Program, Biological and Environmental Science and Engineering Division, King Abdullah University of Science and Technology (KAUST), 23955-6900 Thuwal, Saudi Arabia. ²KAUST Climate and Livability Initiative, King Abdullah University of Science and Technology (KAUST), 23955-6900 Thuwal, Saudi Arabia. ³School of Computer, Data and Information Sciences, University of Wisconsin-Madison, Madison, WI 53715-1007, USA. ⁴Defense and Security, Rabdan Academy, 114646 Abu Dhabi, United Arab Emirates. ✉email: sami.alghamdi@kaust.edu.sa

of human thermal stress is critical for determining the magnitude and extent of human thermal discomfort, identifying thermal stress hotspots, and mitigating potential effects on natural and built environments^{13–15}.

To date, various thermal stress indices have been developed and employed to quantify human thermal stress, including apparent temperature (AT), discomfort index (DI), heat index (HI), humidity index (Humidex), wet-bulb temperature (WBT), wet-bulb-globe temperature (WBGT), the universal thermal climate index (UTCI), etc. All these indices provide insights into the complex interplay between human comfort and environmental factors. According to Yan et al.^{4,12}, thermal indices are designed to quantify the combined effects of various environmental parameters on the human body. Among the above-mentioned indices, UTCI is a widely accepted and reliable indicator of thermal comfort, accounting for both physiological and environmental factors^{13,16,17}. It is an important index used for a comprehensive assessment of human thermal discomfort, by integrating multiple bio-meteorological factors, such as air temperature, relative humidity, wind speed, solar and thermal radiation, human clothing type, and physical activity level^{12,18–20}. The robust and comprehensive assessments of human thermal stress utilizing the UTCI can empower decision-makers to take necessary actions and formulate policy interventions aimed at reducing the adverse impacts of climate change-induced thermal stress in vulnerable regions^{21,22}.

UTCI is currently being used in many parts of the world, to assess changes in human thermal discomfort and other related factors¹⁷. A review study on the use of UTCI found that 60% of the UTCI applications were in outdoor thermal comfort assessment and urban climate and planning studies, while the other 40% of UTCI applications were on climate change-related health impacts, bioclimates, meteorological analyses, climate change research, and tourism²³. In recent years, UTCI has been extensively employed to assess heat-related health risks and identify thermal bioclimatic variability in different parts of Europe^{15,22,24–30}. Similarly, some studies have utilized UTCI to assess observed spatiotemporal changes in human thermal stress in different regions of the Asian continent^{13,31–37}. UTCI is also employed in southern and northern American countries to evaluate the level of human thermal comfort and the potential impacts of heat stress under the current global warming trend^{16,38–41}. Despite being an important index for assessing human thermal comfort, UTCI's application is limited in certain parts of the world, including the Arabian Peninsula (AP). Regions such as AP, which experience extreme heat stress, require urgent studies to assess and measure human thermal discomfort and understand its underlying mechanisms.

AP is characterized by its arid and hot climate⁴². The region has experienced pronounced warming with frequent and intense heat extremes that will continue in the future with more catastrophic implications^{43–46}. To date, a diverse suite of indices has been used to assess observed and projected spatiotemporal changes in human thermal stress in the AP and neighboring regions. For instance, Christidis et al.⁴⁷ used high-risk warming and high-risk days indices to estimate the likelihood of extremely hot days (≥ 50 °C) and heat-related mortalities in the Mediterranean and Middle East regions. Whereas Hajat et al.⁴⁸ applied the AT index to quantify the current and future trends in heat-related mortality in the Middle East and North Africa (MENA) region. In another study, Safieddine et al.⁴³ used a WBT index to analyze current and future human heat stress in the AP, while Kang et al.⁴⁹ applied WBT and dry-bulb temperature indices to estimate future heat stress during the Muslim Pilgrimage (Hajj) season. Similarly, Ahmadalipour and Moradkhani⁵⁰ employed a WBT index to anticipate future heat stress conditions in the MENA region. Some studies also assessed observed changes in human thermal stress in Saudi Arabia, such as Dasari et al.⁵¹ used the DI to analyze the trends and variability of outdoor thermal discomfort, whereas Al-Bouwarthan et al.⁵² employed WBGT to determine the exposure of construction workers to heat stress.

El Niño–Southern Oscillation (ENSO) is a recurring climate pattern involving changes in the temperature of surface waters in the central and eastern tropical Pacific Ocean, which includes three phases: El Niño, La Niña, and neutral^{53,54}. The El Niño phase is associated with the anomalous warm surface water accumulation in the central and eastern Pacific Ocean, the La Niña phase conversely represents the contrary with anomalously cool water in the central and eastern Pacific Ocean^{55,56}. The neutral phase occurs in between El Niño and La Niña events, with sea surface temperatures (SST) and atmospheric conditions returning to near-average levels. Both El Niño and La Niña phases interact with the overlying atmospheric circulation, which leads to various global impacts such as changes in rainfall patterns, droughts, and flooding. ENSO indices' correlations with monthly mean global precipitation and surface temperature reveal the ENSO3.4 and relative ENSO3.4 indices as the strongest for capturing ENSO's global precipitation impact. Conversely, the Nino4 and Nino3.4 indices excel in capturing ENSO's influence on surface temperature, with the Modoki index being the weakest⁵⁷. Researchers in the past have identified different geographical regions in the Pacific Ocean where the SST anomalies as a precursor to ENSO evolution with a broader global implication. The notable indices include ENSO3.0, 3.4, and 4.0. ENSO3.0 (5N–5S, 150W–90W) was initially considered the key region for monitoring and predicting the ENSO and coupled ocean–atmosphere interactions, but the scientists discovered that this area lies further west, and hence ENSO3.4 became more favorable^{53,57}. The ENSO3.4 index (5N–5S, 170W–120W) uses a 5-month running mean, and El Niño or La Niña events are defined when the Niño 3.4 SSTs exceed ± 0.4 °C for a period of six months or more. ENSO4.0 (5N–5S, 160E–150W) is in the central Pacific Ocean and exhibits less variance than the rest of the indices and monitors the eastward propagation of the ENSO.

Though the previously mentioned studies focused on evaluating human thermal stress in the MENA region using various indices, there is very limited literature available regarding the utilization of UTCI for assessing human thermal stress in the AP region. To date, only two studies applied UTCI for human thermal assessment in the AP region^{58,59}; however, these studies were limited to a specific country, i.e., United Arab Emirates (UAE) and Saudi Arabia, and did not cover the whole AP region. Moreover, none of these studies have used the newly developed high-resolution gridded ERA5-HEAT (Human thERmAl comfOrT) dataset, which includes multiple human thermal stress indices, including UTCI⁶⁰. Given these limitations, the present study employs ERA5-HEAT data to evaluate observed spatiotemporal changes in human thermal stress based on UTCI from 1979 to 2022.

In addition, the study explores the interplay between the UTCI indices and the El Niño-Southern Oscillation (ENSO) indices in the AP region. The study findings provide valuable insights for developing effective measures to mitigate human thermal stress and its associated adverse consequences in the region.

Study area

Arabian Peninsula (AP) is a vast and significant geographic region located in Southwest Asia, with geographical coordinates of 12°–32° North latitudes and 34°–60° East longitudes (Fig. 1). AP is the world’s largest peninsula, with an estimated area of 3.2 million km², covering seven countries: Bahrain, Kuwait, Oman, Qatar, Saudi Arabia, the UAE, and Yemen (Fig. 1a). The peninsula is surrounded by major water bodies from multiple sides: the Persian Gulf to the northeast, the Red Sea to the west, the Gulf of Aden to the southwest, the Arabian Sea to the south, and the Gulf of Oman to the southeast. The region has diverse topography, including deserts, mountains, plains, and coastal regions. The Rub’al Khali (Empty Quarter) is one of the largest continuous sand deserts in the world, covering an estimated area of 650,000 km², which is a significant portion of the peninsula’s southern region. The Hijaz and Asir mountain ranges run along the western coast, with some peaks exceeding 3000 m, and they are the highest elevated points in the peninsula (Fig. 1b). The climate of AP is arid to semi-arid, with high annual temperatures and limited precipitation, which make it one of the most vulnerable regions to climate change. The region exhibits spatiotemporal variability in temperature distribution, with a relatively colder climate in the northern parts, a hotter climate in the southern parts, and a moderate climate in the coastal areas. Generally, summers are extremely hot, with maximum temperature ranging from 40 to 50 °C during the daytime, whereas winters are milder, with minimum temperature varying from 8.57 to 10 °C during the nighttime. In AP, precipitation is generally low, with most of the areas receiving less than 100 mm of rainfall annually.

Data and methods

Data

The ERA5 is the fifth and latest version of the European Centre for Medium-Range Weather Forecasts (ECMWF) reanalysis gridded products. Among the ECMWF reanalysis datasets, the ERA5-HEAT, developed by Di Napoli

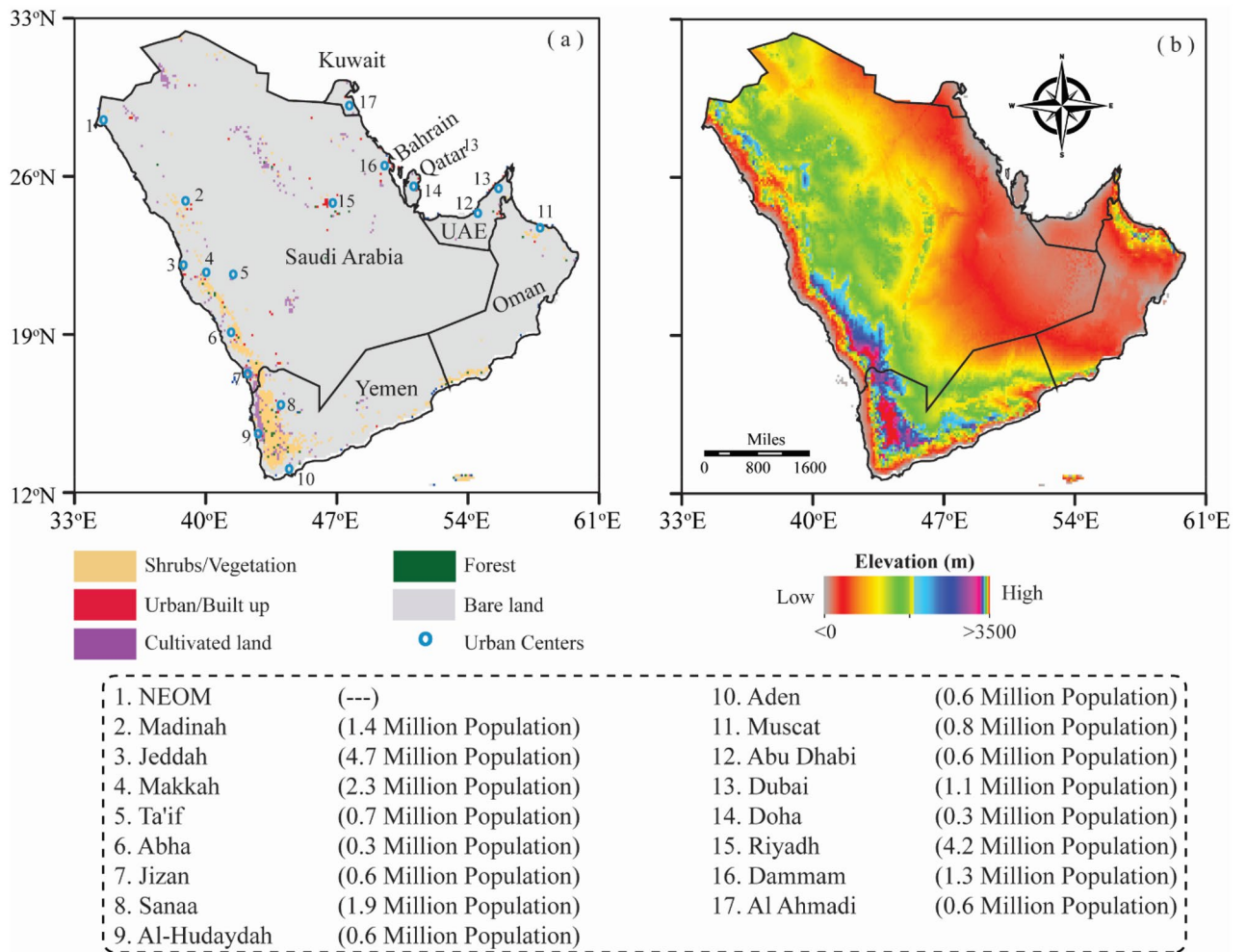


Figure 1. Topographic map of the Arabian Peninsula (AP); (a) land cover classes, the AP member countries, the major urban centers and their respective population, and (b) digital elevation model (DEM) (This figure was created in ArcGIS 10.8).

et al.⁶⁰, is a comprehensive gridded climatic data consisting of various thermal comfort indices, including UTCI. The ERA5-HEAT data are validated against global synoptic stations data, where the UTCI dataset exhibits robust performance, with correlation coefficients exceeding 0.6 (0.80 ± 0.13) at most of the global stations and ranging from 0.9 to 1 in the AP region. Similarly, the root-mean-square error averages 5.2 ± 2.5 °C globally and varies from 0 to 5 °C in the AP region. ERA5-HEAT is an hourly dataset, with a horizontal resolution of $0.25^\circ \times 0.25^\circ$, spanning from 1979 to the present date. In this study, we calculated the daily minimum ($UTCI_{min}$), maximum ($UTCI_{max}$), and mean ($UTCI_{mean}$) UTCI values to assess spatiotemporal changes in daily human thermal discomfort in the AP region for the period 1979–2022. Here the “human thermal discomfort” refers to the feeling or sensation of being too hot or too cold, due to the interaction between environmental conditions and the human body’s temperature regulation²⁰. The ERA5-HEAT data are freely available for public use on the Copernicus Climate Data Store (CDS) portal, which is a part of the Copernicus Climate Change Service (C3S), regulated by ECMWF (<https://cds.climate.copernicus.eu/cdsapp#!/dataset/derived-utci-historical?tab=overview>).

To explore the relationships between the ENSO and UTCI indices in AP, the study also used the monthly time series of three different types of ENSO indices, including ENSO3.0, ENSO3.4, and ENSO4.0. The use of three different ENSO indices aims to understand the complex nature of ENSO’s effects, and its regional variability, providing a holistic insight into the diverse ways ENSO influences thermal comfort in the peninsula. The ENSO indices data are obtained from the National Center for Atmospheric Research (NCAR) for the period 1979–2022 (<https://psl.noaa.gov/data/climateindices/list/>).

Methods

Calculation of UTCI and its classes

To date, more than 100 different indices have been developed to thoroughly assess human thermal discomfort, including the UTCI. In this study, we preferred the use of UTCI over other indices because it is one of the widely used and reliable thermal comfort indicators that integrate both physiological and environmental factors^{13,16,17}. Moreover, it is used as a biometeorology index to characterize and predict human thermal sensation based on a combination of multiple meteorological variables⁶¹. As a human heat exchange model, it is often applied to study the interplay between human health and meteorological factors^{12,18–20}. UTCI is based on an operational procedure that employs a sixth-order polynomial regression approximation equation⁶². In ERA5-HEAT, the UTCI is computed using 2-m air temperature (T_a), mean radiant temperature (MRT), humidity (RH), and wind speed (w) from the ECMWF ERA5 reanalysis, whereas the radiation element was used to calculate the MRT⁶⁰. The mathematical equation of UTCI is as follows (Eq. 1):

$$UTCI(T_a, MRT, w, RH) = T_a + offset(T_a, MRT, w, RH) \quad (1)$$

where T_a is the 2-m air temperature (°C), MRT is the mean radiant temperature (°C), w is the 10-m wind speed (m/s), and RH is the relative humidity (%). Despite its effectiveness, the UTCI calculation has some limitations, including the requirement of the T_a within the range of -50 to 50 °C, $MRT-T_a$ within the range of -30 to 70 °C, and 10-m wind speed should not exceed 17 m/s. More details about the processing and computational procedures of the ERA5-HEAT data are provided by Di Napoli et al.⁶⁰. The AP climate is within these ranges; therefore, the application of the UTCI is suitable in this region.

According to the human body’s thermal physiological response corresponding to the model’s comfort standards, the UTCI values are typically categorized into ten thermal stress levels^{13,21}. Further insights into these UTCI stress categories and their associated physiological conditions can be found in the work of Bröde et al.⁶². Given the prevalent hot tropical climate of the peninsula and the substantial warming observed in recent decades^{63,64}, we considered only six thermal stress categories, primarily representing hot conditions in the study region. The selected human thermal stress categories along with their corresponding physiological conditions are presented in Table 1.

ENSO indices

The three ENSO indices include ENSO3.0, 3.4, and 4.0, which are a representation of the Pacific SST evolution with circumglobal circulations, indirectly affecting the AP’s temperature variability^{65–67}. These indices used here represent an optimal approach to map different phases of the Pacific SST and its relationship with the UTCI indices in the AP.

S. no	UTCI (°C) range	Stress category	Thermal perception
1	0–9	Slight cold stress	Cold
2	9–26	No thermal stress	Comfortable
3	26–32	Moderate heat stress	Warm
4	32–38	Strong heat stress	Hot
5	38–46	Very strong heat stress	Hottish
6	>46	Extreme heat stress	Torrid

Table 1. UTCI categories and their corresponding physiological conditions.

Statistical analysis

The study employed various statistical techniques to determine spatiotemporal changes in human thermal discomfort in the study region. The non-parametric Sen's slope estimator (SSE)⁶⁸ test was used to estimate the slope of the trend, while the modified Mann–Kendall (m-MK)⁶⁹ was employed to determine the statistical significance of the trend in UTCI indices and their stress categories during the study period. We preferred these non-parametric tests over other statistical tests as they are simple and robust against outliers and missing values in a time series^{70,71}. Furthermore, these tests are less sensitive to abrupt breaks in a time series and do not require data normalization^{72,73}. More details about SSE and m-MK tests can be found in recent studies^{74,75}. Furthermore, we explored the relationship between ENSO types and UTCI indices using Pearson's correlation test. The 2-tailed Student *t*-test was employed to determine the statistical significance of correlations at the 95% confidence level. We used CDO (Climate Data Operators) version 2.2.0, Matlab (MATrix LABORatory) version R2022b, ArcGIS version 10.8, and GrADS (Grid Analysis and Display System) version grads-2.2.1 for data pre-processing, data analyses, and data visualization.

Results

Spatiotemporal changes in UTCI indices

Figure 2 shows the long-term spatiotemporal changes and trends in $UTCI_{min}$, $UTCI_{max}$, and $UTCI_{mean}$ over AP during 1979–2022. As seen in Fig. 2a–c, the spatial distribution of long-term climatological means of UTCI indices exhibits large variability in AP, with the highest magnitude (20–45 °C) in the southeastern part and southwestern coastal belt, indicating these parts of the AP had experienced considerable thermal stress in recent decades. The southeastern part of the AP is located along the border intersection of Oman, Saudi Arabia, UAE, and Yemen, having a hyper-arid climate and desert topography. Moreover, the southwestern belt of AP includes the major cities of Jeddah, Makkah, Al-Hudaydah, and Aden. Moreover, the central and eastern parts of the AP, mostly encompassing the metropolitan cities of Riyadh, Dammam, Doha, and Al Ahmadi, tend to experience UTCI magnitudes within the range of 10–35 °C. While the northern and northwestern parts experienced the lowest climatological intensity of UTCI indices (0–25 °C) during the study period. In terms of UTCI indices,

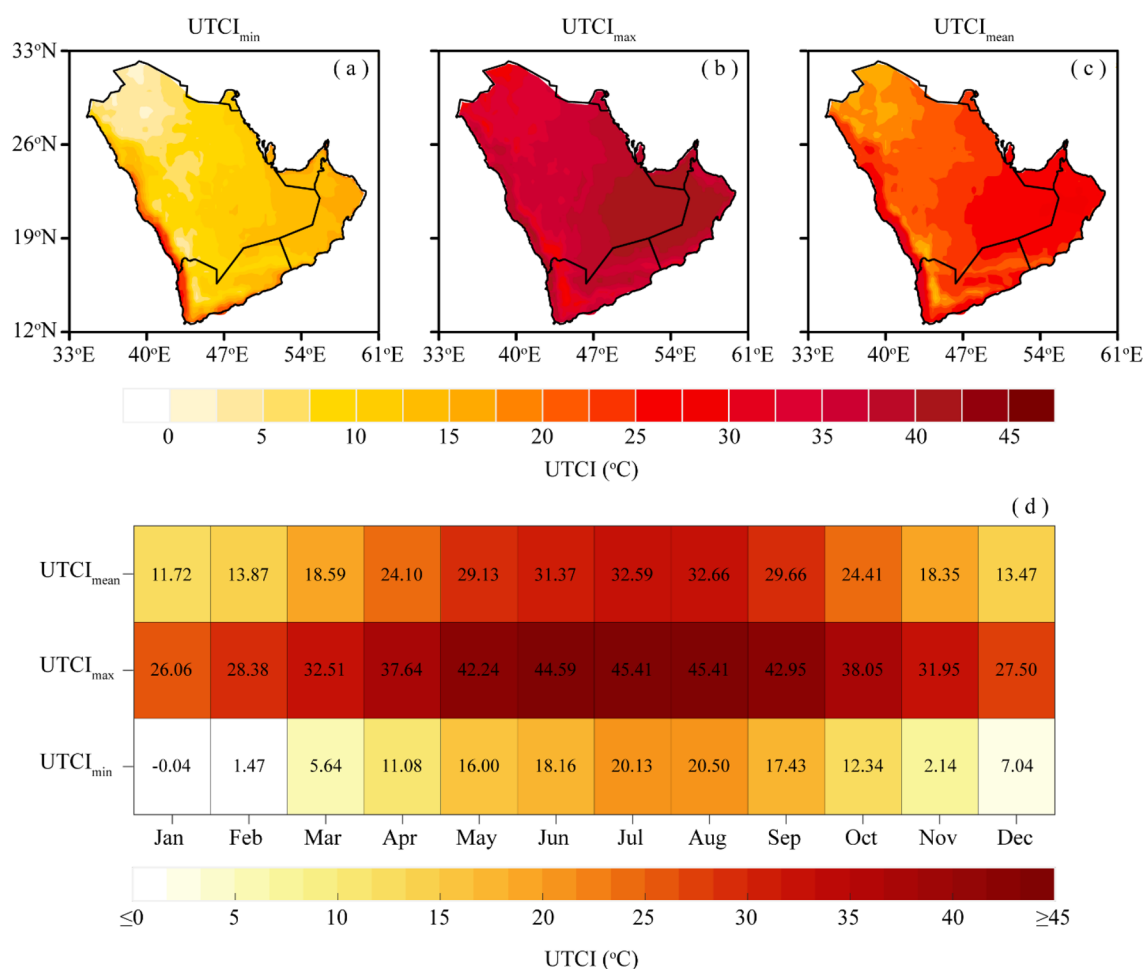


Figure 2. Long-term climatological means of UTCI indices over AP during 1979–2022; (a–c) spatial climatological means of $UTCI_{min}$, $UTCI_{max}$, and $UTCI_{mean}$, respectively, and (d) monthly means of $UTCI_{min}$, $UTCI_{max}$, and $UTCI_{mean}$ (In this figure, panels (a–c) were created in GrADS 2.2.1, while panel (d) was created Matlab R2022b).

the long-term climatological magnitude of $UTCI_{min}$, $UTCI_{max}$, and $UTCI_{mean}$ ranges from 0 to 30 °C, 25 to 45 °C, and 15 to 35 °C, respectively.

As shown in Fig. 2d, the overall intensities of monthly $UTCI_{min}$, $UTCI_{max}$, and $UTCI_{mean}$ range from -0.04 to 20.50 °C, 26.06 to 45.41 °C, and 11.72 to 32.66 °C, respectively. The monthly analyses further show that July and August have the warmest thermal conditions, followed by June, September, and May with observed maximum intensities of 45.41 °C, 44.49 °C, 42.95 °C, and 42.24 °C, respectively. In contrast, January has the coldest thermal conditions, followed by February, March, and December with minimum UTCI intensities of -0.04 °C, 1.47 °C, 5.64 °C, and 7.04 °C, respectively. These results indicate that the AP is under the strong influence of thermal stress during the summer months.

The spatiotemporal trend in UTCI indices over the AP during 1979–2022 is presented in Fig. 3. The rising trend of UTCI indices shows a significant increase in thermal stress with higher spatial variability during the study period (Fig. 3a–c). The southwestern parts of AP, consisting of mountains and coastlines, exhibit a substantial increase of 0.6–0.8 °C/decade in UTCI indices. The central regions of AP also exhibit a notable warming trend in UTCI indices, ranging from 0.4 to 0.6 °C/decade. It is worth mentioning that both the southwestern and central parts of AP comprised some of the several populated cities, including Al-Hudaydah, Sanaa, Abha, Jeddah, Jizan, Makkah, Madinah, and Riyadh. The results further show that the northeastern and southeastern parts of AP experienced a relatively least increasing trend of 0.10–0.30 °C/decade in UTCI indices, which indicates that the stated areas have observed the lowest heat stress during the study period. These include the junction of the Saudi–Yemen–Oman border, and some major coastal metropolitan cities, such as Dammam, Dubai, Abu Dhabi, Muscat, Doha, and Al Ahmadi. Overall, the magnitude and spatial extent of the warming trend are larger in $UTCI_{min}$, followed by $UTCI_{mean}$ and $UTCI_{max}$. As shown in Fig. 3d, the long-term temporal trend in annual anomalies of UTCI indices exhibits a linear increase during the study period. However, this increasing trend became more consistent during 1998 and onward, indicating a transition toward intensified regional climate warming and the emergence of frequent and intense heat extremes in AP. The monotonic trend results reveal

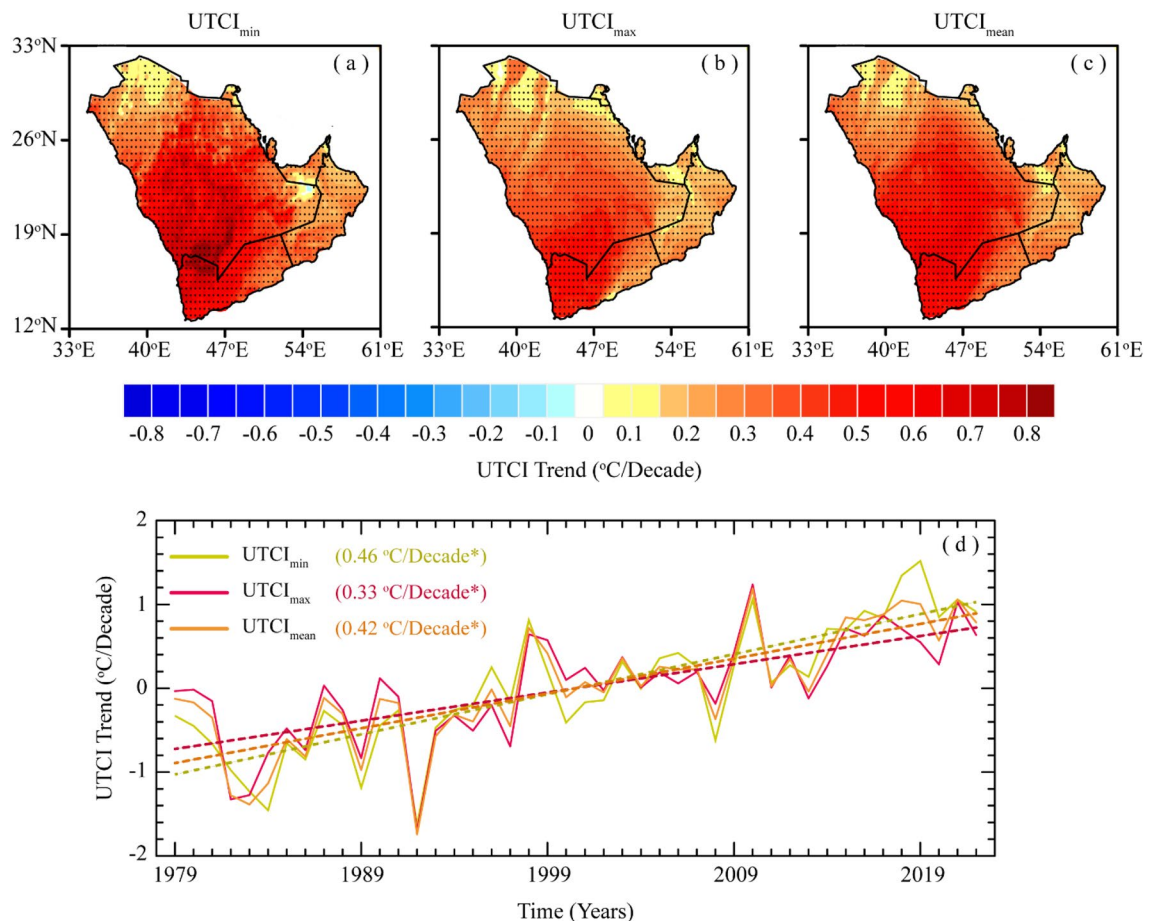


Figure 3. Long-term trends of UTCI indices over AP during 1979–2022; (a–c) spatial trends of $UTCI_{min}$, $UTCI_{max}$, and $UTCI_{mean}$, respectively, and (d) temporal trends of $UTCI_{min}$, $UTCI_{max}$, and $UTCI_{mean}$. The black dots in figures (a–c) indicate that the trend is statistically significant at the 0.05 significance level. The values in Figure (d) represent the monotonic trends of UTCI indices, while the asterisk (*) indicates that the trend is statistically significant at the 0.05 significance level (In this figure, panels (a–c) were created in GrADS 2.2.1, while panel (d) was created Matlab R2022b).

that the $UTCI_{min}$ exhibits the highest significant increasing trend, followed by $UTCI_{mean}$ and $UTCI_{max}$ at the rates of 0.46 °C, 0.42 °C, and 0.33 °C per decade, respectively.

Spatiotemporal changes in UTCI stress categories

Figure 4 depicts the spatial trend of the frequency of UTCI stress categories over AP during 1979–2022. Based on $UTCI_{min}$ and $UTCI_{mean}$ (Fig. 4a,c), a substantial reduction in the number of “slight cold stress” days is evident across most areas of the AP (–1 to –9 days/decade), except for the southern territories where a marginal increase in $UTCI_{min}$ -based “slight cold stress” days is observed (1–4.5 days/decade). It is noteworthy that $UTCI_{max}$ does not signify any instances of “slight cold stress” days during the study period (Fig. 4b), which can be attributed to the consistently higher daily maximum temperatures in the AP that do not fall within the range of “slight cold stress” category throughout the year. Furthermore, the frequency of days falling into the “no thermal stress” category reveals an augmentation of 3–15 days/decade in the southwestern, central, and northwestern regions (Fig. 4d–f). Nonetheless, the magnitude and spatial extent of this increasing trend are more pronounced in $UTCI_{min}$ than in $UTCI_{max}$ and $UTCI_{mean}$. Conversely, the remaining regions of the AP have experienced a decreasing trend in the “no thermal stress” days, with a more notable decline (–12 to –15 days/decade) in $UTCI_{mean}$ observed along the Oman-UAE border (Fig. 4f).

As presented in Fig. 4g–i, the count of days characterized by “moderate heat stress” has risen in the southern, western, and eastern horn of the AP (along the Oman-UAE border), signifying a noticeable shift from the “no thermal stress” to the “moderate heat stress” category. In contrast, the remainder of the AP displays a declining trend, indicating a progression toward higher thermal stress categories. The number of “strong heat stress” days exhibits a visible pattern of increase (15–18 days/decade), with major hotspots in the southwestern and eastern parts of the AP (Fig. 4j–l). However, this upward trend is more prominent in $UTCI_{mean}$ than in $UTCI_{min}$ and $UTCI_{max}$. Importantly, these regions encompass major metropolitan areas, including Jeddah, Madinah, Makkah, NEOM (a newly developing city in western Saudi Arabia), Dammam, and Muscat. Our results further demonstrate that the frequency of “strong heat stress” days, based on $UTCI_{max}$ and $UTCI_{mean}$, is significantly on the rise in the northern and southeastern regions of the AP at a rate of 3–15 days/decade (Fig. 4n,o), with the most substantial trend observed in the inland areas along the Saudi-Oman-Yemen border junction. It is worth noting that “very strong heat stress” days based on $UTCI_{min}$ did not exhibit any discernible trend (Fig. 4m), owing to their lower intensity that does not surpass the recommended thermal thresholds in the study region. Furthermore, our findings reveal that when considering $UTCI_{max}$, the frequency of “extreme thermal stress” days exhibits a general increase across the AP (Fig. 4q), with the most pronounced tendency (3–11 days/decade) observed in the southwestern, central, and eastern regions. These areas encompass major cities, including Jeddah, Makkah, Madinah, NEOM, Jizan, Riyadh, Dammam, Al-Hudaydah, Sanaa, Doha, and Al Ahmadi. Conversely, $UTCI_{min}$ and $UTCI_{mean}$ do not indicate any occurrences of “extreme heat stress” days (Fig. 4p,r), which can be attributed to their lower intensities observed in the AP, falling below the recommended thermal thresholds.

Figure 5 illustrates the spatial distribution of trends in the intensity of UTCI categories over the AP region. Both $UTCI_{min}$ and $UTCI_{mean}$ exhibit an asymmetric pattern of intensity for the “slight cold stress” category, with the most significant increase (0.01–0.20 °C/decade) observed in the central, eastern, southern (Fig. 5a), and southwestern parts of AP (Fig. 5c). This signifies that these regions of AP have experienced a rise in the intensity of “slight cold stress” during the study period. In contrast, $UTCI_{max}$ did not exhibit “slight cold stress” intensity due to higher daily maximum temperatures and lower thresholds for the “slight cold stress” category (Fig. 5b). The increasing tendency of the “no thermal stress” intensity is most pronounced (0.08–0.60 °C/decade) over most of the AP region (Fig. 5d–f), indicating normal climatic conditions during the study period. Some parts of the AP, such as the inland southwestern region along the Saudi–Yemen border have witnessed a decrease in the intensity of the “no thermal stress” category; however, in the case of $UTCI_{max}$ and $UTCI_{mean}$, this decreasing trend shifts to the northwestern, eastern, and southern parts of the peninsula.

Moreover, the intensity of the “moderate heat stress” category exhibits a mixed pattern of increasing and decreasing trends across the AP region (Fig. 5g–i). The $UTCI_{min}$ -based “moderate heat stress” intensity displays a dipole pattern with an increasing trend of 0.01–0.12 °C/decade in the northwestern and southwestern parts of AP. Conversely, the $UTCI_{max}$ -based intensity, while slightly reduced (0.01–0.04 °C/decade), extends over the central and extreme northeastern parts of the peninsula. Notably, the $UTCI_{mean}$ -based “moderate heat stress” intensity reveals a more evident decreasing trend; however, the upper central part of Saudi Arabia and the eastern horn of AP—major parts of Oman and UAE—experienced an increase of 0.01–0.20 °C/decade. The regions with increasing trends in “moderate heat stress” intensity encompass several major urban clusters within the AP, such as Jeddah, Makkah, Riyadh, Dammam, Muscat, Abu Dhabi, and Dubai, underscoring the extent of population exposure to extreme and persistent heat stress in these cities.

The results of all UTCI indices show a positive trend in the intensity of “strong heat stress” over the AP, with the maximum spatial extent in $UTCI_{mean}$, followed by $UTCI_{max}$ and $UTCI_{min}$ (Fig. 5j–l). Both $UTCI_{min}$ and $UTCI_{max}$ show an increasing trend of 0.01–0.24 °C/decade in the northern and southern parts. However, the magnitude of this increasing trend is more pronounced in $UTCI_{min}$, while its spatial extent is greater in $UTCI_{max}$. In contrast, the intensity of the $UTCI_{mean}$ -based “strong heat stress” exhibits the highest increasing trend over major parts of AP; however, this increasing trend is strongly concentrated (0.12–0.28 °C/decade) in the central AP, indicating a significant presence of thermal discomfort in these areas. Additionally, the intensity of “very strong heat stress” based on the $UTCI_{max}$ and $UTCI_{mean}$ indices revealed a rising trend (0.01–0.24 °C/decade) in the western, southern, and eastern parts of the peninsula (Fig. 5n,o). However, the $UTCI_{min}$ -based intensity of “very strong heat stress” does not exhibit any significant trend (Fig. 5m), likely due to lower values of daily $UTCI_{min}$, falling below the recommended thresholds for the “very strong heat stress” category. Furthermore, based on $UTCI_{max}$ (Fig. 5q), a significant increase is observed in the intensity of “extreme heat stress” over major

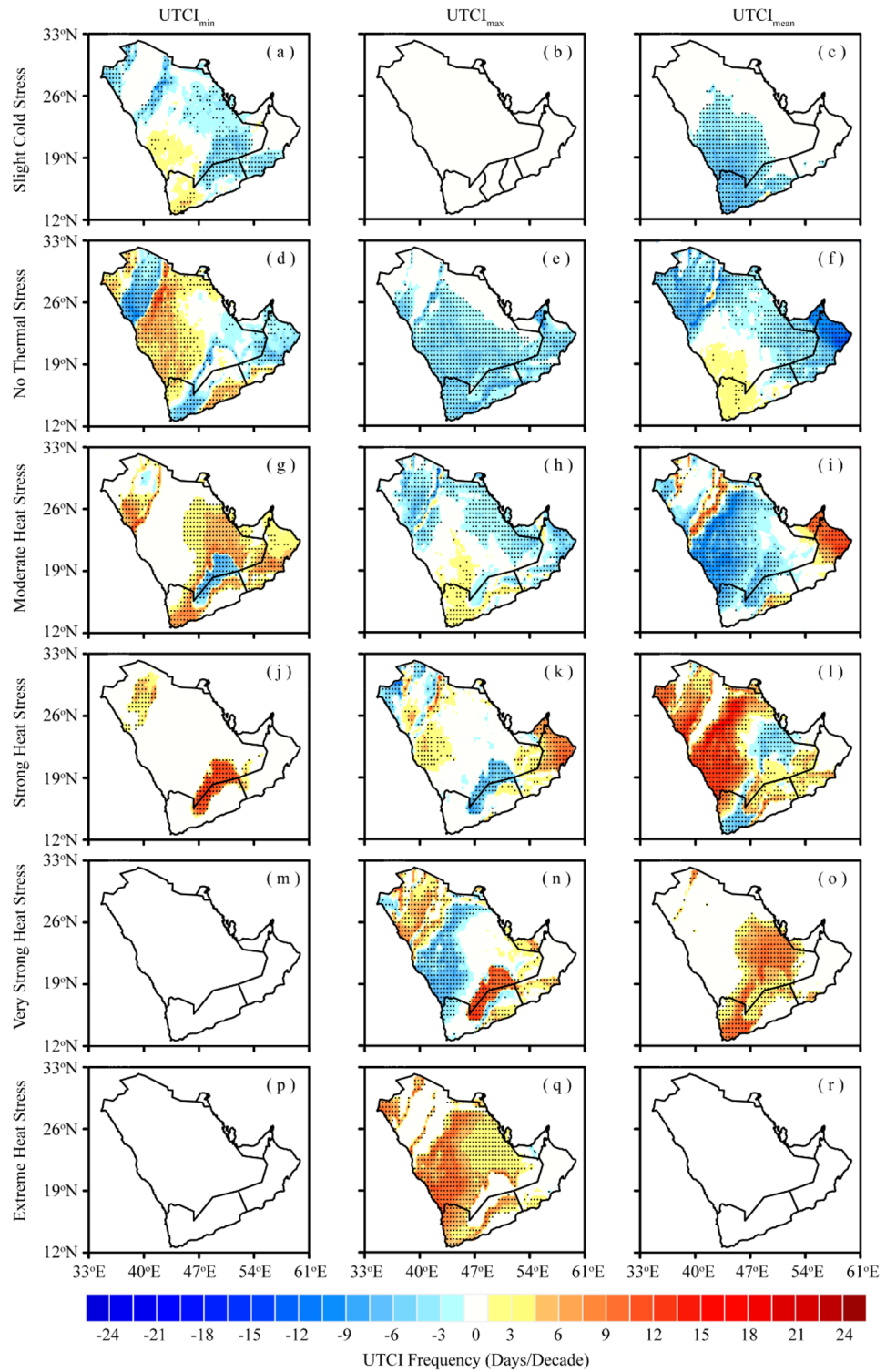


Figure 4. Spatial trends in the frequency of UTCI stress categories over AP during 1979–2022; (a–c) Slight cold stress, (d–f), No thermal stress, (g–i) Moderate heat stress, (j–l), Strong heat stress, (m–o) Very strong heat stress, and (p–r) Extreme heat stress. The black dots indicate that the trend is statistically significant at the 0.05 significance level (This figure was created in GrADS 2.2.1).

parts of the AP, with substantial intensification (0.16–0.44 °C/decade) in the major urban clusters, including Jeddah, Makkah, Jizan, Riyadh, Dammam, Al-Hudaydah, Sanaa, and Doha. In contrast, the $UTCI_{min}$ and $UTCI_{mean}$

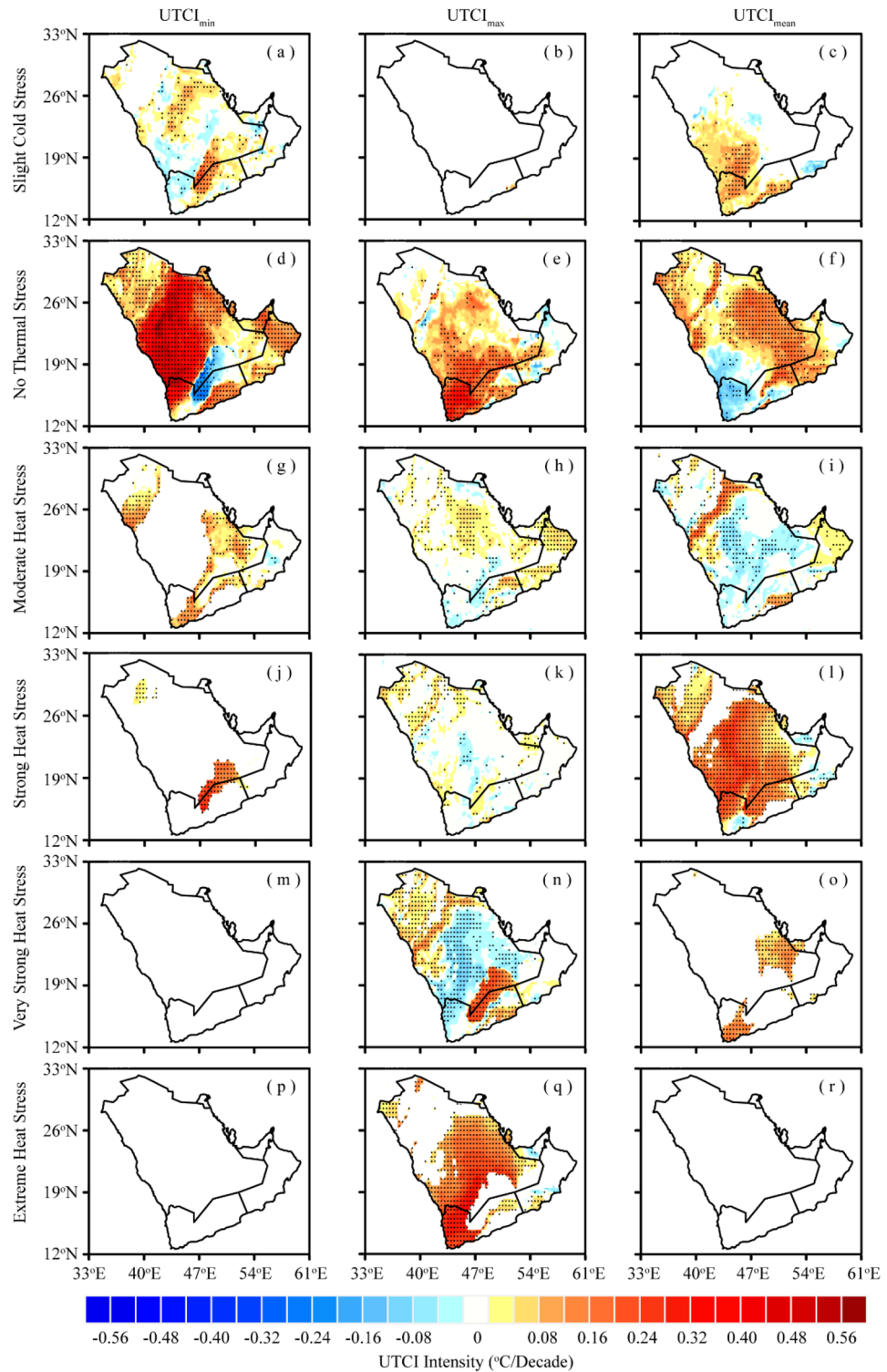


Figure 5. Spatial trends in the intensity of UTCI stress categories over AP during 1979–2022; (a–c) Slight cold stress, (d–f) No thermal stress, (g–i) Moderate heat stress, (j–l) Strong heat stress, (m–o) Very strong heat stress, and (p–r) Extreme heat stress. The black dots indicate that the trend is statistically significant at the 0.05 significance level (This figure was created in GrADS 2.2.1).

indices do not signify any “extreme heat stress” magnitude (Fig. 5p,r), due to their lower intensities falling below the recommended thermal thresholds.

Figure 6 depicts the temporal patterns of annual anomalies and linear trends in the frequency and intensity of UTCI stress classes over AP during 1979–2022. In terms of frequency, the number of days with “slight cold stress”, “no thermal stress”, and “moderate heat stress” decreased (Fig. 6a–c), while those of “strong heat stress”, “very strong heat stress”, and “extreme heat stress” increased significantly during the study period (Fig. 6d–f). Irrespective of their counterparts, the frequency of UTCI_{max}-based “very strong heat stress” days decreased (Fig. 6e), while the number of days with “no thermal stress” and “moderate heat stress” based on UTCI_{min} increased during the study period (Fig. 6b,c). The temporal distribution of annual anomalies reveals a sharp increase in the frequency of human thermal stress during 1998 and onward, indicating a shift towards a hotter climate for a prolonged period in the study region. As shown in Table 2, the outcomes of the monotonic trend indicate that the number of “slight cold stress”, “no thermal stress”, and “moderate heat stress days” has decreased in the range of -0.564 to -1.040 , -1.091 to -1.133 , and -0.491 to -1.014 days/decade, respectively. Whereas the frequency of “strong heat stress”, “very strong heat stress”, and “extreme heat stress” has increased at the rates of 0.052 – 2.334 , and 2.072 days/decade, respectively.

In terms of intensity (Fig. 6g–l), most of the stress categories exhibited an increasing trend, suggesting that the peninsula has been dominated by significant thermal discomfort during the study period. The temporal pattern of annual anomalies shows that the intensity of thermal heat stress classes sharply increased in the later years of the period. The increasing intensity of the thermal stress categories indicates the consistent occurrence of intense heat stress in the study region. A suite of the literature revealed that the major parts of AP have witnessed several episodes of heat extremes over the past few decades^{63,76,77}, affirming the findings of this study. Given the monotonic trend (Table 3), the intensity of the “slight cold stress”, “no thermal stress”, “moderate heat stress”, “strong heat stress”, “very strong heat stress”, and “extreme heat stress” has increased at the rates of 0.009 – 0.032 , 0.037 – 0.298 , 0.016 – 0.028 , 0.022 – 0.120 , 0.003 – 0.050 , and 0.117 °C/decade, respectively, indicating their evolution into higher stress categories with consistent and considerable thermal stress.

Role of ENSO on UTCI Amplification

Figure 7 shows the spatial correlation between the annual mean of daily UTCI_{min}, UTCI_{max}, and UTCI_{mean} and three ENSO indices, including ENSO3.0, ENSO3.4, and ENSO4, representing the Pacific Ocean surface temperature in the eastern, central, and western parts of the Pacific during 1979–2022, respectively. The correlation between the UTCI_{min} and the three ENSO indices shows a dipole pattern with negative (< -0.50) values in the eastern AP and positive values (0.60) in the southwestern parts. The UTCI_{max} and the ENSO indices show a similar correlation pattern, but the geographical spread of the negative correlation shows that the eastern Pacific surface temperature (ENSO3.0 and ENSO3.4) has widespread effects on the UTCI_{max} than the western Pacific Ocean surface temperature where a strong dipole is evident. The UTCI_{mean} shows a similar correlation as observed for UTCI_{max} with ENSO indices, except for the ENSO4.0, which has a significant effect on the dipole pattern of this correlation. The ENSO and UTCI indices relationship over the AP shows two distinct patterns, including the dipole effect of the western Pacific forcing (ENSO4.0) which is more prominent for the UTCI_{min} than for the UTCI_{max} and UTCI_{mean}. The eastern Pacific ENSO indices (ENSO3.0 and ENSO3.4), on the other hand, have a significant negative relationship with UTCI_{max} and UTCI_{mean} values, implying that a positive mode of the ENSO in the eastern Pacific would produce below-normal human thermal stress and vice versa. The same is evident for the ENSO4.0 but the dipole pattern shows a regionally varying effect.

Discussion

Global warming-induced climate change coupled with population expansion and rapid urbanization has amplified human thermal stress in urban environments, which could adversely affect the comfort level of the local population. This study aims to assess spatiotemporal changes in human thermal stress over the AP region and its urban centers using multiple UTCI indices for the period 1979–2022. The results of the study show that the southeastern and southwestern parts of AP have higher climatological values of UTCI indices, suggesting that these parts have experienced considerable thermal stress in recent decades. This further highlights the level of vulnerability of these regions to climate change and its heat extremes. The higher intensity of UTCI indices in these parts of AP can be attributed to their distinct location, complex climate, and diverse topography, as the southeastern region has a hyper-arid climate with desert topography, high temperatures, and limited precipitation⁶³, while the southwestern region is located along the coast of Red Sea, having hot-humid climate and complex topographic features. On the other hand, the northern and northwestern parts of AP have the lowest climatological mean of UTCI indices, which can be linked to the onset of the cold Siberian High, the passage of the Mediterranean cyclones and the fronts, and the formation of the Shamal winds⁷⁸.

In terms of the annual cycle, the study region has the warmest thermal conditions in July and August, followed by June, September, and May, while the coldest thermal conditions are in January and February, followed by March, and December. These results indicate that the AP region is under the strong (weak) influence of thermal stress during the summer (winter) months. The results closely align with the findings of recent studies^{13,37,79}, which reported similar warm (cold) thermal conditions during the summer (winter) months in different parts of the world. It is worth mentioning that both the warm and cold thermal months reflect the summer and winter seasons of the AP region, where the summers are extremely hot, while the winters are relatively mild. During the summer season, the AP climate is often hot-humid—daytime temperatures sometimes exceed 50 °C with high humidity, while in winters, the climate is relatively milder with cold breezes at nighttime—temperatures remain less than 20 °C with the least heat stress.

In terms of the long-term trend, most of the AP parts, including the southwestern, central, northeastern, and southeastern parts have experienced a significant increase in UTCI indices, suggesting pronounced thermal stress in these regions during the study period. It is worth mentioning that these parts of AP comprised some of

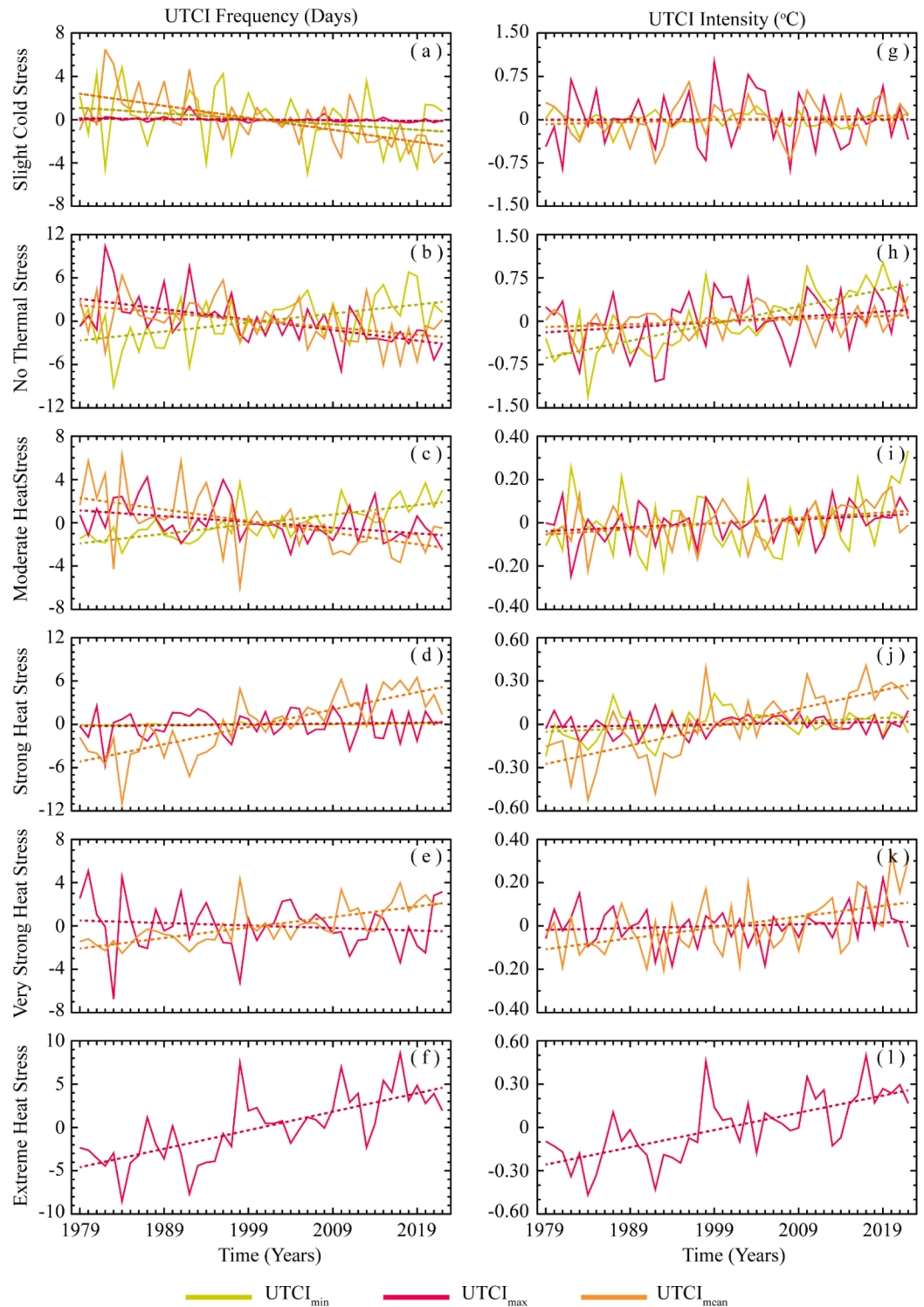


Figure 6. Temporal trends in the frequency and intensity of UTCI stress categories over AP during 1979–2022; (a–f) frequency and (g–l) intensity of UTCI indices. The solid lines in different colors indicate the annual anomalies of UTCI indices, while the dotted lines indicate their respective linear trends (This figure was created in Matlab R2022b).

the major global urban centers. This increasing trend of UTCI indices can be attributed to various natural and anthropogenic factors, including geographical features, land-sea interactions, topographical influences, population expansion, rapid urbanization, and urban heat island effects^{5,63,80,81}. Moreover, the UTCI indices exhibited

Stress category	Frequency (days/decade)		
	UTCI _{min}	UTCI _{max}	UTCI _{mean}
Slight cold stress	-0.564	-0.052	-1.040
No thermal stress	1.203	-1.133	-1.091
Moderate heat stress	0.832	-0.491	-1.014
Strong heat stress	0.064	0.052	2.334
Very strong heat stress	-	-0.365	0.921
Extreme heat stress	-	2.072	-

Table 2. Monotonic temporal trend in the frequency of UTCI stress categories. The bold values indicate that the trend is statistically significant at the 0.05 significance level.

Stress category	Intensity (°C/decade)		
	UTCI _{min}	UTCI _{max}	UTCI _{mean}
Slight cold stress	-0.002	0.009	0.032
No thermal stress	0.298	0.078	0.037
Moderate heat stress	0.026	0.016	0.028
Strong heat stress	0.022	0.008	0.120
Very strong heat stress	-	0.003	0.050
Extreme heat stress	-	0.117	-

Table 3. Monotonic temporal trend in the intensity of UTCI stress categories. The bold values indicate that the trend is statistically significant at the 0.05 significance level.

an asymmetric warming trend in the AP, with a higher magnitude and larger spatial extent in UTCI_{min}, followed by UTCI_{mean} and UTCI_{max}, which can be attributed to the sharp increase in daily minimum temperature to maximum and mean temperatures and their related extremes^{64,77,81}. Such heterogeneous patterns of minimum, maximum, and mean temperatures have been observed in AP and other parts of the world, which confirm our current findings^{13,31,32,58,59}.

Furthermore, the long-term temporal anomalies exhibit a linear increase during the study period, with a sharp increase during the late 1990s and onward, which indicates a shift toward a more intensified regional climate and pronounced heat stress in recent decades in AP. Similar results are reported by several studies, stating that over the last two decades, many parts of the AP region have experienced the highest surface temperature and intense heat extremes, with increased health-related risks^{63,82}. The World Meteorological Organization (WMO) also declares that the last two decades (2001–2020) as the hottest ones in the world's history^{83,84}. The warming trend in UTCI indices and resultant thermal stress in the urban centers of AP is consistent with broader global climate change trends, which may have implications for local human populations. These findings are of paramount importance as they provide a comprehensive overview of the spatial distribution and increasing trend of thermal stress in AP, highlighting regions of particular concern for diverting climate change adaptation and mitigation measures.

We further studied the frequency and intensity of the UTCI categories and revealed the southwestern, northern, and central parts of the AP experienced a significant increase in the frequency and intensity of “strong heat stress”, “very strong heat stress”, and “extreme heat stress” categories. Importantly, these regions encompass major metropolitan areas, including Jeddah, Madinah, Makkah, NEOM, Dammam, Muscat, Jizan, Riyadh, Al-Hudaydah, Sanaa, Doha, Al Ahmadi, and the inland areas along the Saudi-Oman-Yemen border junction. The increasing frequency and intensity of thermal stress implies that these cities have experienced frequent and intense episodes of extreme heat stress during the study period. This suggests that the urban population in the AP has experienced frequent and intense heat stress, potentially leading to heat-related health issues, such as heat exhaustion and heat stroke^{49,50,76}. Similar to UTCI indices, the temporal distribution of annual anomalies of UTCI stress categories reveals a sharp increase in the frequency and intensity of human thermal stress during 1998 and onward, indicating a shift towards a persistent hot climate in the peninsula during the study period, which could have adverse impacts on the comfort level of the local population. Recently, several studies reported similar hot climate patterns, with substantial impacts on the local population in the peninsula and neighboring regions^{50,85–87}.

Overall, the rise in the frequency and intensity of extreme thermal stress in the AP can be attributed to its distinct geographical location, multifaceted topography, complex climatic conditions, regional and global atmospheric systems, urban development, and population growth^{63,88}. It is important to mention that the cities located in the southwestern and eastern parts of the AP have hot-humid climates due to their proximity to the Red Sea and the Arabian Sea, which acts as a major source of moisture and water vapor for humid weather in the coastal areas^{89,90}. The increase in the number and magnitude of heat stress episodes in hot-humid cities is also driven by rapid urbanization and population expansion, particularly in the AP region^{63,91}. Whereas the

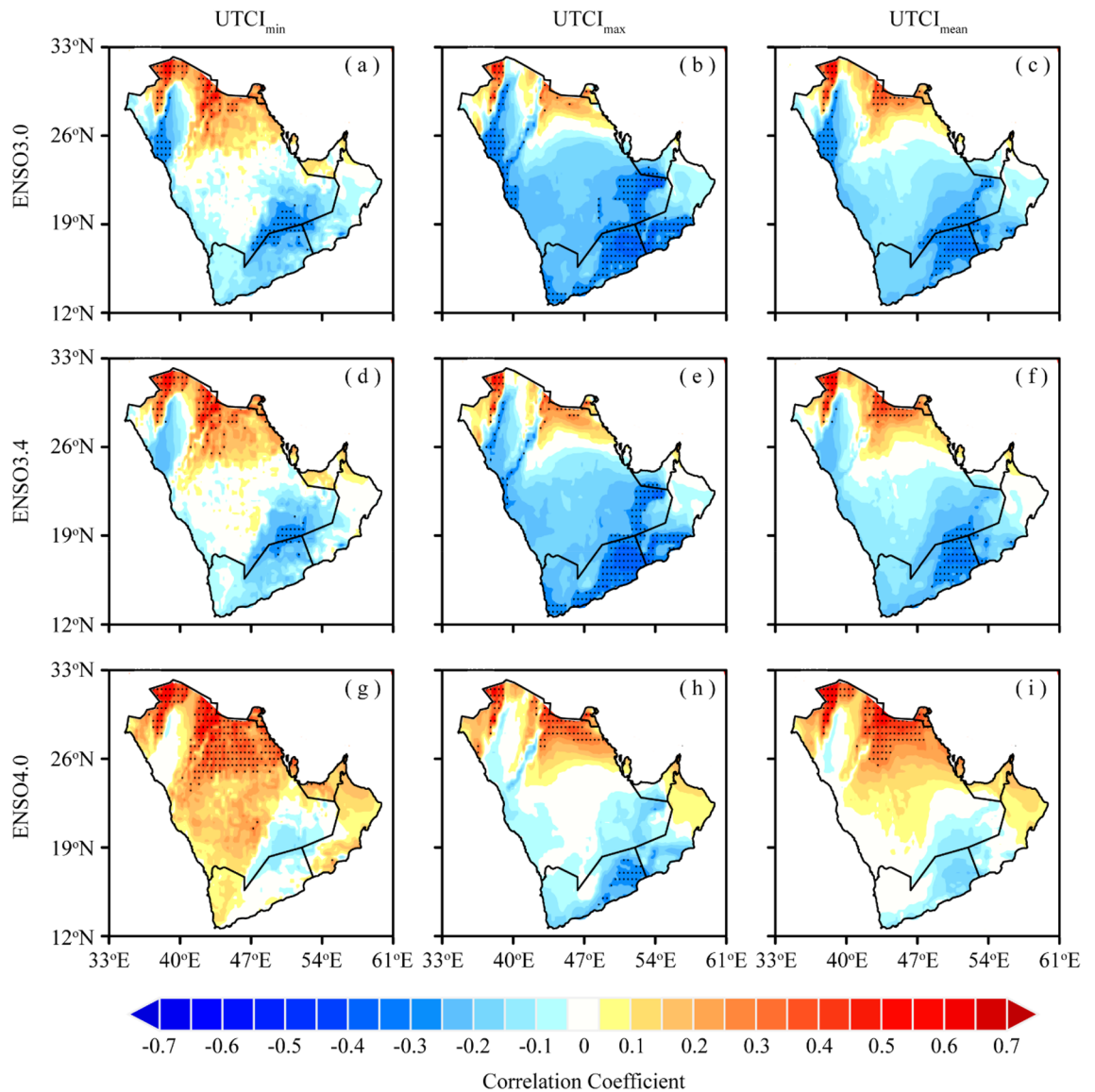


Figure 7. Spatial correlation between UTCI and ENSO indices over AP during 1979–2022; (a–c) ENSO3.0, (d–f) ENSO3.4, and (g–i) ENSO4.0. The black dots indicate that the correlation is statistically significant at the 0.05 significance level (This figure was created in GrADS 2.2.1).

southern cities of Jizan, Al-Hudaydah, and Sanaa are located at higher altitudes, the increasing number of heat stress days in these cities can be linked to elevation-dependent warming—a phenomenon in which high altitude areas experience relatively higher warming than those of the low-lying plains^{92,93}. The central and inland cities have a typical arid-hot climate and are located in or near the Rub’ al Khali, which is an integral part of the Arabian desert. Consequently, policymakers and city planners should consider these trends when formulating strategies to mitigate the adverse impacts of heat stress on the local population in AP and other regions with similar climatic characteristics.

The ENSO and UTCI indices relationship over the AP shows two distinct patterns, including the dipole effect of the western Pacific forcing (ENSO4.0), which is more prominent for the $UTCI_{min}$ than for the $UTCI_{max}$ and $UTCI_{mean}$. The eastern Pacific ENSO indices (ENSO3.0 and ENSO3.4), on the other hand, have a significant negative relationship with $UTCI_{max}$ and $UTCI_{mean}$ values, implying that a positive mode of the ENSO in the eastern Pacific would produce below-normal human thermal stress and vice versa in the AP region. Similar results were previously reported for temperature anomalies as a consequence of the ENSO-induced circumglobal changes in the circulations^{1,2}. The same is evident for the ENSO4.0 but the dipole pattern shows a regionally varying effect. The mechanism of the dipole pattern for the eastern Pacific and $UTCI_{min}$ could be related to the ENSO-driven monsoon circulation that affects the South Asian monsoon through controlling the zonal easterlies and hence a negative relationship with the eastern parts of AP and positive relationship with the western AP^{72,73,94,95}. The eastern Pacific on the other hand appeared to have widespread global effects and thus its positive mode could affect the Indian Ocean basin-wide forcing and the overall thermal stress regime of the AP region^{96–99}.

Conclusion

The study analyzed spatiotemporal changes in human thermal stress categories and their characteristics and investigated the correlation between the UTCI and ENSO indices in the AP during the period 1979–2022. The results of the study show that the major urban centers in the southwestern and central parts of the AP have experienced a significant increase in UTCI-based human thermal stress, indicating the predominance of frequent, intense, and prolonged human thermal discomfort during the study period. These urban centers include Jeddah, Jizan, Makkah, Madinah, Riyadh, Abha, NEOM, Riyadh, Dammam, Abu Dhabi, Dubai, Doha, Muscat, Al-Hudaydah, and Sanaa. This increase in the frequency and intensity of thermal discomfort in AP's urban centers can be attributed to their distinct geographical locations, complex climatic conditions, regional and global atmospheric systems, urbanization, and population growth. The results further demonstrate a consistent increase in human thermal stress and its frequency and intensity over the years, particularly from 1998 onwards, indicating a transition towards a hotter climate with frequent and intense heat extremes for a prolonged period in the study region. The correlation between the UTCI and ENSO indices shows a dipole pattern with a positive pattern in the southwestern and a negative pattern in the eastern AP, which modulates the thermal stress regime in AP. The ENSO evolution in the eastern equatorial Pacific (ENSO3.0 and ENSO3.4) significantly affects the $UTCI_{max}$ and $UTCI_{min}$ whereas the western Pacific (ENSO4.0) has significant control over the $UTCI_{mean}$ pattern in a much larger area compared to the eastern Pacific indices. The results of the study call for particular attention to public health and well-being in urban areas, particularly vulnerable groups, such as the elderly, children, women, disabled individuals, laborers, and marginalized populations. The findings emphasized the need for policymakers to consider these trends for effective climate change adaptation and mitigation strategies to address the growing impact of heat stress on the AP's urban population. Furthermore, the results urged that city and urban planners need to carefully strategize and develop future cities and towns in areas, which are less vulnerable to the adverse effects of climate change, particularly heat stress.

Data availability

The datasets used in this study are publicly available at their given links. The ERA5-HEAT data can be obtained from the Copernicus Climate Data Store (CDS) website of the Copernicus Climate Change Service (C3S) and the European Centre for Medium-Range Weather Forecasts (ECMWF) (<https://cds.climate.copernicus.eu/cdsapp#!/dataset/derived-utci-historical?tab=overview>). The ENSO indices time series data can be accessed from the National Center for Atmospheric Research (NCAR) website (<https://psl.noaa.gov/data/climateindices/list/>).

Code availability

The codes used for data processing can be provided on request to the corresponding author.

Received: 1 November 2023; Accepted: 16 February 2024

Published online: 17 February 2024

References

- Zhao, Q., Lian, Z. & Lai, D. Thermal comfort models and their developments: A review. *Energy Built Environ.* **2**, 21–33 (2021).
- Rupp, R. F., Vásquez, N. G. & Lamberts, R. A review of human thermal comfort in the built environment. *Energy Build* **105**, 178–205 (2015).
- Andrić, I., Koc, M. & Al-Ghamdi, S. G. A review of climate change implications for built environment: Impacts, mitigation measures and associated challenges in developed and developing countries. *J. Clean. Prod.* **211**, 83–102 (2019).
- Yang, C. & Zhao, S. Synergies or trade-offs between surface urban heat island and hot extreme: Distinct responses in urban environments. *Sustain. Cities Soc.* **101**, 105093 (2024).
- Sachindra, D. A., Ullah, S., Zaborski, P., Nowosad, M. & Dobek, M. Temperature and urban heat island effect in Lublin city in Poland under changing climate. *Theor. Appl. Climatol.* **151**, 667–690 (2023).
- Mohajerani, A., Bakaric, J. & Jeffrey-Bailey, T. The urban heat island effect, its causes, and mitigation, with reference to the thermal properties of asphalt concrete. *J. Environ. Manag.* **197**, 522–538 (2017).
- Vahmani, P. & Ban-Weiss, G. A. Impact of remotely sensed albedo and vegetation fraction on simulation of urban climate in WRF-urban canopy model: A case study of the urban heat island in Los Angeles. *J. Geophys. Res.: Atmos.* **121**, 1511–1531 (2016).
- Fang, W. *et al.* Hotter and drier climate made the Mediterranean Europe and Northern Africa region a shrubbier landscape. *Oecologia* **197**, 1111–1126 (2021).
- Dunne, J. P., Stouffer, R. J. & John, J. G. Reductions in labour capacity from heat stress under climate warming. *Nat. Clim. Change* **3**, 563–566 (2013).
- Teixeira, E. I., Fischer, G., Van Velthuizen, H., Walter, C. & Ewert, F. Global hot-spots of heat stress on agricultural crops due to climate change. *Agric. For. Meteorol.* **170**, 206–215 (2013).
- Schwingshackl, C., Sillmann, J., Vicedo-Cabrera, A. M., Sandstad, M. & Aunan, K. Heat stress indicators in CMIP6: Estimating future trends and exceedances of impact-relevant thresholds. *Earths Future* **9**, 1–17 (2021).
- Yan, Y., Xu, Y. & Yue, S. A high-spatial-resolution dataset of human thermal stress indices over South and East Asia. *Sci. Data* **8**, 1–14 (2021).
- Ullah, S. *et al.* Characteristics of human thermal stress in South Asia during 1981–2019. *Environ. Res. Lett.* **17**, 104018 (2022).
- Sylla, M. B., Faye, A., Giorgi, F., Diedhiou, A. & Kunstmann, H. Projected heat stress under 1.5 °C and 2 °C global warming scenarios creates unprecedented discomfort for humans in West Africa. *Earths Future* **6**, 1029–1044 (2018).
- Błażejczyk, A., Błażejczyk, K., Baranowski, J. & Kuchcik, M. Heat stress mortality and desired adaptation responses of healthcare system in Poland. *Int. J. Biometeorol.* **62**, 307–318 (2018).
- Bröde, P., Krüger, E. L., Rossi, F. A. & Fiala, D. Predicting urban outdoor thermal comfort by the Universal Thermal Climate Index UTCI—A case study in Southern Brazil. *Int. J. Biometeorol.* **56**, 471–480 (2012).
- Błażejczyk, K. UTCI—10 years of applications. *Int. J. Biometeorol.* **65**, 1461–1462 (2021).
- Jendritzky, G., de Dear, R. & Havenith, G. UTCI—Why another thermal index?. *Int. J. Biometeorol.* **56**, 421–428 (2012).
- Havenith, G. *et al.* The UTCI-clothing model. *Int. J. Biometeorol.* **56**, 461–470 (2012).
- Fiala, D., Havenith, G., Bröde, P., Kampmann, B. & Jendritzky, G. UTCI-Fiala multi-node model of human heat transfer and temperature regulation. *Int. J. Biometeorol.* **56**, 429–441 (2012).

21. Blazejczyk, K., Epstein, Y., Jendritzky, G., Staiger, H. & Tinz, B. Comparison of UTCI to selected thermal indices. *Int J Biometeorol* **56**, 515–535 (2012).
22. Krzyżewska, A., Wereski, S. & Dobek, M. Summer UTCI variability in Poland in the twenty-first century. *Int. J. Biometeorol.* **65**, 1497–1513 (2021).
23. Krüger, E. L. Literature Review on UTCI Applications. in *Applications of the Universal Thermal Climate Index UTCI in Biometeorology* 23–65 (Springer, 2021). https://doi.org/10.1007/978-3-030-76716-7_3.
24. Novak, M. Use of the UTCI in the Czech Republic. *Geogr. Pol.* **86**, 21–28 (2013).
25. Urban, A. & Kysely, J. Comparison of UTCI with other thermal indices in the assessment of heat and cold effects on cardiovascular mortality in the Czech Republic. *Int. J. Environ. Res. Public Health* **11**, 952–967 (2014).
26. Németh, Á. Changing thermal bioclimate in some Hungarian cities. *Acta Climatol. Chorol.* **44–45**, 93–101 (2011).
27. Bleta, A., Nastos, P. T. & Matzarakis, A. Assessment of bioclimatic conditions on Crete Island, Greece. *Environ. Change* **14**, 1967–1981 (2014).
28. Nastos, P. T. & Matzarakis, A. The effect of air temperature and human thermal indices on mortality in Athens, Greece. *Theor. Appl. Climatol.* **108**, 591–599 (2012).
29. Matzarakis, A., Muthers, S. & Rutz, F. Application and comparison of UTCI and pet in temperate climate conditions. *Finisterra* **49**, 21–31 (2014).
30. Burkart, K. *et al.* Modification of heat-related mortality in an elderly urban population by vegetation (Urban Green) and proximity to water (Urban Blue): Evidence from Lisbon, Portugal. *Environ. Health Perspect.* **124**, 927–934 (2016).
31. Kyaw, A. K., Hamed, M. M. & Shahid, S. Spatiotemporal changes in Universal Thermal Climate Index over South Asia. *Atmos. Res.* **292**, 106838 (2023).
32. Roshan, G. R., Ghanghermeh, A. A. & Kong, Q. Spatial and temporal analysis of outdoor human thermal comfort during heat and cold waves in Iran. *Weather Clim. Extremes* **19**, 58–67 (2018).
33. Zeng, Y. L. & Dong, L. Thermal human biometeorological conditions and subjective thermal sensation in pedestrian streets in Chengdu, China. *Int. J. Biometeorol.* **59**, 99–108 (2015).
34. Park, J., Kim, Y. & Oh, I. Factors affecting heat-related diseases in outdoor workers exposed to extreme heat. *Ann. Occup. Environ. Med.* **29**, 4–9 (2017).
35. Seo, Y. & Honjo, T. Thermal stress in Tokyo and Sapporo during the 2020 Olympics period. *J. Environ. Inf. Sci.* **2021**, 29–36 (2021).
36. Vinogradova, V. Using the Universal Thermal Climate Index (UTCI) for the assessment of bioclimatic conditions in Russia. *Int. J. Biometeorol.* **65**, 1473–1483 (2021).
37. Jacobs, C. *et al.* Patterns of outdoor exposure to heat in three South Asian cities. *Sci. Environ.* **674**, 264–278 (2019).
38. Emerton, R. *et al.* Predicting the unprecedented: Forecasting the June 2021 Pacific Northwest heatwave. *Weather* **77**, 272–279 (2022).
39. Katal, A. *et al.* Outdoor heat stress assessment using an integrated multi-scale numerical weather prediction system: A case study of a heatwave in Montreal. *Sci. Total Environ.* **865**, 161276 (2023).
40. Provençal, S., Bergeron, O., Leduc, R. & Barrette, N. Thermal comfort in Quebec City, Canada: Sensitivity analysis of the UTCI and other popular thermal comfort indices in a mid-latitude continental city. *Int. J. Biometeorol.* **60**, 591–603 (2016).
41. Lucchese, J. R., Mikuri, L. P., De Freitas, N. V. S. & Andreasi, W. A. Application of selected indices on outdoor thermal comfort assessment in Midwest Brazil. *Int. J. Energy Environ.* **7**, 2076–2909 (2016).
42. Ajjur, S. B. & Al-Ghamdi, S. G. Evapotranspiration and water availability response to climate change in the Middle East and North Africa. *Clim. Change* **166**, 28 (2021).
43. Safieddine, S., Clerboux, C., Clarisse, L., Whitburn, S. & Eltahir, E. A. B. Present and future land surface and wet bulb temperatures in the Arabian Peninsula. *Environ. Res. Lett.* **17**, 044029 (2022).
44. Saeed, F., Schlessner, C.-F. & Almazroui, M. From Paris to Makkah: Heat stress risks for Muslim pilgrims at 1.5 °C and 2 °C. *Environ. Res. Lett.* **16**, 024037 (2021).
45. Ajjur, S. B. & Al-Ghamdi, S. G. Global hotspots for future absolute temperature extremes from CMIP6 models. *Earth Space Sci.* **8**, e2021EA001817 (2021).
46. McCabe, M. *et al.* *Climate Futures Report: Saudi Arabia in a 3-Degree Warmer World.* (2023). <https://doi.org/10.25718/KAUST-8XY63>.
47. Christidis, N., Mitchell, D. & Stott, P. A. Rapidly increasing likelihood of exceeding 50 °C in parts of the Mediterranean and the Middle East due to human influence. *NPJ Clim. Atmos. Sci.* **6**, 45 (2023).
48. Hajat, S., Proestos, Y., Araya-Lopez, J.-L., Economou, T. & Lelieveld, J. Current and future trends in heat-related mortality in the MENA region: A health impact assessment with bias-adjusted statistically downscaled CMIP6 (SSP-based) data and Bayesian inference. *Lancet Planet Health* **7**, e282–e290 (2023).
49. Kang, S., Pal, J. S. & Eltahir, E. A. B. Future heat stress during muslim pilgrimage (Hajj) projected to exceed “extreme danger” levels. *Geophys. Res. Lett.* **46**, 10094–10100 (2019).
50. Ahmadalipour, A. & Moradkhani, H. Escalating heat-stress mortality risk due to global warming in the Middle East and North Africa (MENA). *Environ. Int.* **117**, 215–225 (2018).
51. Dasari, H. P., Desamsetti, S., Langodan, S., Viswanadhapalli, Y. & Hoteit, I. Analysis of outdoor thermal discomfort over the Kingdom of Saudi Arabia. *Geohealth* **5**, e2020GH000370 (2021).
52. Al-Bouwarthan, M., Quinn, M. M., Kriebel, D. & Wegman, D. H. Assessment of heat stress exposure among construction workers in the hot desert climate of Saudi Arabia. *Ann. Work Expo. Health* **63**, 505–520 (2019).
53. Wang, C., Deser, C., Yu, J.-Y., DiNezio, P. & Clement, A. El Niño and Southern Oscillation (ENSO): A Review. 85–106 (2017). https://doi.org/10.1007/978-94-017-7499-4_4.
54. Timmermann, A. *et al.* El Niño–Southern oscillation complexity. *Nature* **559**, 535–545 (2018).
55. Wang, S., Huang, J., He, Y. & Guan, Y. Combined effects of the Pacific decadal oscillation and El Niño–Southern oscillation on global land dry–wet changes. *Sci. Rep.* **4**, 6651 (2014).
56. El Mysak, L. A. Niño, interannual variability and fisheries in the Northeast Pacific Ocean. *Can. J. Fish. Aquat. Sci.* **43**, 464–497 (1986).
57. Wang, Z., Wu, D., Chen, X. & Qiao, R. ENSO indices and analyses. *Adv. Atmos. Sci.* **30**, 1491–1506 (2013).
58. Kishta, M., Robaa, S. M., Wahab, M. M. A. & Abadla, Z. A. Spatial distribution of outdoor thermal human comfort in the UAE. *World J. Adv. Res. Rev.* **13**, 043–049 (2022).
59. Odnoletkova, N. & Patzek, T. W. Data-driven analysis of climate change in Saudi Arabia: Trends in temperature extremes and human comfort indicators. *J. Appl. Meteorol. Climatol.* <https://doi.org/10.1175/JAMC-D-20-0273.1> (2021).
60. Di Napoli, C., Barnard, C., Prudhomme, C., Cloke, H. L. & Pappenberger, F. ERA5-HEAT: A global gridded historical dataset of human thermal comfort indices from climate reanalysis. *Geosci. Data J.* **8**, 2–10 (2021).
61. Bröde, P. Issues in UTCI Calculation from a Decade’s Experience. in *Applications of the Universal Thermal Climate Index UTCI in Biometeorology* 13–21 (Springer, 2021). https://doi.org/10.1007/978-3-030-76716-7_2.
62. Bröde, P. *et al.* Deriving the operational procedure for the Universal Thermal Climate Index (UTCI). *Int. J. Biometeorol.* **56**, 481–494 (2012).
63. Zittis, G. *et al.* Climate change and weather extremes in the Eastern Mediterranean and Middle East. *Rev. Geophys.* **60**, e2021RG000762 (2022).

64. Jaber, S. M., Abu-Allaban, M. M. & Sengupta, R. Spatial and temporal patterns of indicators of climate change and variability in the Arab world in the past four decades. *Sci. Rep.* **13**, 15145 (2023).
65. Huang, Y., Liu, X., Yin, Z. & An, Z. Global impact of ENSO on dust activities with emphasis on the key region from the Arabian Peninsula to Central Asia. *J. Geophys. Res.: Atmos.* **126**, e2020JD034068 (2021).
66. Attada, R. *et al.* Surface air temperature variability over the Arabian Peninsula and its links to circulation patterns. *Int. J. Climatol.* **39**, 445–464 (2019).
67. Almazroui, M., Rashid, I. U., Saeed, S. & Islam, M. N. ENSO influence on summer temperature over Arabian Peninsula: role of mid-latitude circulation. *Clim. Dyn.* **53**, 5047–5062 (2019).
68. Sen, P. K. Estimates of the regression coefficient based on Kendall's Tau. *J. Am. Stat. Assoc.* **63**, 1379–1389 (1968).
69. Hamed, K. H. & Rao, R. A. A modified Mann–Kendall trend test for autocorrelated data. *J. Hydrol. (Amst.)* **204**, 182–196 (1998).
70. Xie, W., Zhou, B., You, Q., Zhang, Y. & Ullah, S. Observed changes in heat waves with different severities in China during 1961–2015. *Theor. Appl. Climatol.* **141**, 1529–1540 (2020).
71. Ullah, S. *et al.* Spatiotemporal changes in global aridity in terms of multiple aridity indices: An assessment based on the CRU data. *Atmos. Res.* **268**, 105998 (2022).
72. Rebi, A. *et al.* Spatiotemporal precipitation trends and associated large-scale teleconnections in Northern Pakistan. *Atmosphere (Basel)* **14**, 871 (2023).
73. Ullah, W. *et al.* An increasing trend in daily monsoon precipitation extreme indices over Pakistan and its relationship with atmospheric circulations. *Front. Environ. Sci.* **11** (2023).
74. Abbas, A. *et al.* Projection of precipitation extremes over South Asia from CMIP6 GCMs. *J. Arid Land* **15**, 274–296 (2023).
75. Hussain, A. *et al.* Spatiotemporal temperature trends over homogenous climatic regions of Pakistan during 1961–2017. *Theor. Appl. Climatol.* **153**, 397–415 (2023).
76. Waha, K. *et al.* Climate change impacts in the Middle East and Northern Africa (MENA) region and their implications for vulnerable population groups. *Reg. Environ. Change* **17**, 1623–1638 (2017).
77. Almazroui, M., Islam, M. N., Dambul, R. & Jones, P. D. Trends of temperature extremes in Saudi Arabia. *Int. J. Climatol.* **34**, 808–826 (2014).
78. Patlakas, S., Flocas, K. & Kallos, Regional climatic features of the Arabian Peninsula. *Atmosphere (Basel)* **10**, 220 (2019).
79. Hamed, M. M., Kyaw, A. K., Nashwan, M. S. & Shahid, S. Spatiotemporal changes in Universal Thermal Climate Index in the Middle East and North Africa. *Atmos. Res.* **295**, 107008 (2023).
80. Almazroui, M. & Hasanean, H. M. Saudi Arabia's summer surface air temperature and its association with circulation patterns. *Int. J. Climatol.* **40**, 5727–5743 (2020).
81. Donat, M. G. *et al.* Changes in extreme temperature and precipitation in the Arab region: Long-term trends and variability related to ENSO and NAO. *Int. J. Climatol.* **34**, 581–592 (2014).
82. Perkins-Kirkpatrick, S. E. & Lewis, S. C. Increasing trends in regional heatwaves. *Nat. Commun.* **11**, 3357 (2020).
83. WMO. *State of the Global Climate 2020*. (2021).
84. Shen, L. *et al.* Performance evaluation of ERA5 extreme precipitation in the Yangtze River Delta, China. *Atmosphere (Basel)* **13**, 1416 (2022).
85. Weber, T. *et al.* Analysis of compound climate extremes and exposed population in Africa under two different emission scenarios. *Earths Future* **8**, 1–19 (2020).
86. Ullah, S. *et al.* Future population exposure to daytime and nighttime heat waves in South Asia. *Earths Future* **10**, 1–16 (2022).
87. Ullah, S. *et al.* Climate change will exacerbate population exposure to future heat waves in the China-Pakistan economic corridor. *Weather Clim. Extremes* **40**, 100570 (2023).
88. Salimi, M. & Al-Ghamdi, S. G. Climate change impacts on critical urban infrastructure and urban resiliency strategies for the Middle East. *Sustain. Cities Soc.* **54**, 101948 (2020).
89. Pathak, A., Ghosh, S., Kumar, P. & Murtugudde, R. Role of oceanic and terrestrial atmospheric moisture sources in intraseasonal variability of Indian summer monsoon rainfall. *Sci. Rep.* **7**, 1–11 (2017).
90. Ullah, S. *et al.* Daytime and nighttime heat wave characteristics based on multiple indices over the China-Pakistan economic corridor. *Clim. Dyn.* **53**, 6329–6349 (2019).
91. Kalnay, E. & Cai, M. Impact of urbanization and land-use change on climate. *Nature* **423**, 528–531 (2003).
92. You, Q. *et al.* Elevation dependent warming over the Tibetan Plateau: Patterns, mechanisms and perspectives. *Earth Sci. Rev.* **210**, 1–19 (2020).
93. You, Q., Zhang, Y., Xie, X. & Wu, F. Robust elevation dependency warming over the Tibetan Plateau under global warming of 1.5 °C and 2 °C. *Clim. Dyn.* **53**, 2047–2060 (2019).
94. Ullah, W. *et al.* Large-scale atmospheric circulation patterns associated with extreme monsoon precipitation in Pakistan during 1981–2018. *Atmos. Res.* **253**, 105489 (2021).
95. Hussain, A. *et al.* Assessment of precipitation extremes and their association with NDVI, monsoon and oceanic indices over Pakistan. *Atmos. Res.* **292**, 106873 (2023).
96. Cherchi, A. *et al.* The influence of tropical Indian Ocean SST on the Indian summer monsoon. *J. Clim.* **20**, 3083–3105 (2007).
97. Chu, J.-E. *et al.* Future change of the Indian Ocean basin-wide and dipole modes in the CMIP5. *Clim. Dyn.* **43**, 535–551 (2014).
98. Hu, J. & Duan, A. Relative contributions of the Tibetan Plateau thermal forcing and the Indian Ocean Sea surface temperature basin mode to the interannual variability of the East Asian summer monsoon. *Clim. Dyn.* **45**, 2697–2711 (2015).
99. Hussain, A. *et al.* Ocean–atmosphere circulation coherences associated with temperature increase in Pakistan. *Environ. Res. Lett.* **18**, 094028 (2023).

Acknowledgements

The authors would like to acknowledge the developers of the ERA5-HEAT data for producing and making available their dataset. The authors also thank the National Center for Atmospheric Research (NCAR) for providing the ENSO data.

Author contributions

All the authors contributed to conceptualizing and designing the study. S.U., A.A., and W.U. provided the research idea, gathered data, prepared the figures, and validated the results. S.G.A. supervised and coordinated the research team, revised the article, and provided the required resources. All the authors consented to publish the paper.

Competing interests

The authors declare no competing interests.

Additional information

Correspondence and requests for materials should be addressed to S.G.A.-G.

Reprints and permissions information is available at www.nature.com/reprints.

Publisher's note Springer Nature remains neutral with regard to jurisdictional claims in published maps and institutional affiliations.



Open Access This article is licensed under a Creative Commons Attribution 4.0 International License, which permits use, sharing, adaptation, distribution and reproduction in any medium or format, as long as you give appropriate credit to the original author(s) and the source, provide a link to the Creative Commons licence, and indicate if changes were made. The images or other third party material in this article are included in the article's Creative Commons licence, unless indicated otherwise in a credit line to the material. If material is not included in the article's Creative Commons licence and your intended use is not permitted by statutory regulation or exceeds the permitted use, you will need to obtain permission directly from the copyright holder. To view a copy of this licence, visit <http://creativecommons.org/licenses/by/4.0/>.

© The Author(s) 2024